Stochastic Particle Barcoding for Single-Cell Tracking and Multiparametric Analysis

*M. Castellarnau, G. L. Szeto, H.-W. Su, T. Tokatlian, J. C. Love, D. J. Irvine, and J. Voldman**

This study presents stochastic particle barcoding (SPB), a method for tracking cell identity across bioanalytical platforms. In this approach, single cells or small collections of cells are co-encapsulated within an enzymatically-degradable hydrogel block along with a random collection of fluorescent beads, whose number, color, and position encode the identity of the cell, enabling samples to be transferred in bulk between single-cell assay platforms without losing the identity of individual cells. The application of SPB is demonstrated for transferring cells from a subnanoliter protein secretion/phenotyping array platform into a microtiter plate, with re-identification accuracies in the plate assay of 96±2%. Encapsulated cells are recovered by digesting the hydrogel, allowing subsequent genotyping and phenotyping of cell lysates. Finally, a model scaling is developed to illustrate how different parameters affect the accuracy of SPB and to motivate scaling of the method to thousands of unique blocks.

1. Introduction

There is an increasing appreciation that understanding biological decision-making requires tracing information flow through cells, which necessitates assaying multiple measures of genotype and phenotype on hundreds or thousands of individual cells. Additionally, there is inherent functional heterogeneity among cell types, among single cells within defined cell types, and even among clonal populations;[1,2] this heterogeneity holds significant promise for elucidating the mechanisms of many processes in health and disease[3–5] and thus motivates the development of assays applicable to sparse populations of cells (defined as single cells or groups of 2–10 cells).[6,7] Novel platforms that have been developed to achieve this goal often center on microfluidic approaches, such as arrays of micro/nano/picoliter-volume wells,[8–10] microchambers,[11–14] and emulsion-based droplet technologies.[15–17] Ideally, these novel single-cell assays would be used sequentially with more traditional methods (e.g., single-cell RT-PCR, DNASeq and RNASeq, proteomics) on the same individual cells to more completely link cell signaling, phenotype, and responsiveness. However, an outstanding challenge for many novel analytical platforms is the ability to retain the identity of individual cells within a population, particularly while transferring them from modern bioanalytical assays such as microfluidic devices to standardized platforms (e.g., microtiter plates) for further analysis. Current solutions to this challenge include cell-by-cell transfer (e.g., capillary-based micromanipulators),[9,18] fluorescent labeling,[19–21] barcoding particles (e.g., hydrogel encoded particles,[22] semiconductor tags),[23,24] or molecular labels.[23–25] Cell-by-cell manipulation requires direct access to cells and typically has limited throughput due to its serial nature. Fluorescent labeling is successfully used for highly multiplexed detection

M. Castellarnau, G. L. Szeto, H.-W. Su, T. Tokatlian, J. C. Love, D. J. Irvine, J. Voldman
Massachusetts Institute of Technology
77 Massachusetts Avenue, Cambridge, MA 02139, USA
E-mail: voldman@mit.edu
G. L. Szeto, J. C. Love, D. J. Irvine
The Ragon Institute of MGH, MIT, and Harvard
400 Technology Square, Cambridge, MA 02139, USA
D. J. Irvine
Howard Hughes Medical Institute
4000 Jones Bridge Road, Chevy Chase, MD 20815, USA

DOI: 10.1002/smll.201401369

of bioanalytes,[26,27] but its application to cell tracking is constrained by the limits of spectral multiplexing and prior knowledge of cell states/labels to generate a labeling scheme to track cells. Furthermore, various labeling approaches or dyes may alter cellular function or phenotype. Barcoding particles have struggled with coding depth[28,29] and/or the challenge of co-localizing the coding particle with the cell, while molecular labels typically destroy the cell during reading, or compromise potential barcode depth in exchange for non-destructive detection, e.g., fluorescence.[23] An ideal method for cell tracking would be 1) scalable for hundreds to thousands of cells, 2) selectively able to target a subpopulation based on parameters such as function, 3) non-destructive/non-disruptive to cells to allow multiple assays to be correlated, and 4) allow transfer of cells between arbitrary single-cell or multi-cell assay platforms.

We have developed a method for tracking cells that uses as its code random combinations of beads in a cell-containing hydrogel block; by integrating this method with a previously developed microwell array, we provide the potential to screen cells based on phenotypes or functions (e.g., circulating tumor cells or antibody secretion). The hydrogel blocks comprised a polyethylene glycol diacrylate (PEGDA) photopolymer with an enzymatically cleavable peptide linker. The identity of each block (and its contents) was assigned and tracked using a stochastic barcode generated by the number, color, and position of fluorescently colored beads entrapped in the block matrix. By making the parameter space (number of colors, positions, bead sizes) of the random code sufficiently large, we minimized the probability of two blocks having overlapping codes. We applied this method to track cells during en masse transfer of cells from arrays of subnanoliter wells (MWA) into microtiter plates. We showed that collagenase–mediated digestion of cell-laden blocks enables non-destructive recovery of viable tracked cells and successful nucleic acid isolation and assays. Finally, we used Monte Carlo simulations to assess the scalability of this method up to 1000's of uniquely coded blocks with arbitrary accuracy. This method now enables tracking of sparse populations of cells across platforms and utilizing previous processes developed for the microwell array platform, enabling the potential connection of genotype, phenotype, and function.

2. Results and Discussion

2.1. Overview of Stochastic Particle Barcoding

In tracking sparse populations across platforms, we sought a method that had high coding depth (up to thousands of unique codes), that would not require physical access to the cells as required by pre-generated barcodes (e.g., fluorescent dyes), but rather allowed codes to be built onto the cells in situ, and that could be used with diverse bioanalytical platforms. The main concept underlying stochastic particle barcoding (SPB) is a code that is randomly built around the cells via an in situ polymerization step. This code is determined by the number, fluorescent color, and position of beads photopolymerized around a set of cells, which allows identity tracking of cells across analytical platforms.

Here, we implemented this method within a novel platform (MWA) that enables dynamic interrogation of cell function where subsequent transfer of cells to a microtiter plate is useful for integrative analysis (**Figure 1**). In this workflow, an initial assay on individual cells is carried out in the MWA (an example analysis is discussed further below). Once this initial assay is performed, a prepolymer solution (poly(ethylene glycol) diacrylate (PEGDA) or a digestible acrylate-PEG-peptide-PEG-acrylate, macromonomers commonly used for cell encapsulation in tissue engineering,[30] containing a suspension of beads of different fluorescent colors (red, green and blue) is pipetted onto the MWA (Figure 1A). We sealed the device with a glass slide that is coated with a pH-sensitive sacrificial layer, poly(2,2-dimethoxy nitrobenzyl methacrylate-*r*-methyl methacrylate-*r*-poly(ethylene glycol) methacrylate) (PDMP).[31–33] Sealing enables the generation of discrete hydrogel blocks. Then, we flip the device to allow the beads to settle; sedimentation of the beads onto the plane of the wells in contact with the sealing glass slide simplifies subsequent imaging-based identification and image processing steps. Next, we photopolymerized either the entire array or individual microwells to lock in the codes, comprising the random distributions of number, fluorescent color, and 2D location of the beads at the boundary of the microwells with the glass slide (Figure 1B). Once the code was locked, we removed the glass slide from the MWA and imaged the cell-encapsulating hydrogel blocks (Figure 1C). This step yielded the first set of images, from which a code was assigned to each block corresponding to known positions in the MWA. We then dissolved the PDMP sacrificial layer to detach the blocks (Figure 1D) and transferred them into eppendorf tubes (Figure 1E). The blocks were finally transferred into a microtiter plate by serial dilution (Figure 1F) to obtain a single hydrogel block per well. Then, we imaged the blocks again to read the code and used this second set of images to match blocks in the microtiter plate with those from the MWA, identifying individual cells from the original assay (Figure 1G). Finally, we can degrade the hydrogel blocks by adding an enzyme, such as collagenase, to recover encapsulated cells for further analysis (Figure 1H, and Supporting Information Videos S1).

2.2. Block Matching

We recovered block identity by matching two sets of block images: one taken after photopolymerization and one after plate transfer. Instead of performing computations on the block images themselves, we instead extracted the code information (bead number, color, and position) and performed computations on the reduced data set. We first segmented the images to find the outline of each block and the associated beads, recording their color and 2D position (**Figure 2**A, and Supporting Information Figure S1). For matching blocks, we only considered beads detected inside or on the block perimeter; the position and color of each bead was stored in a matrix for every block.

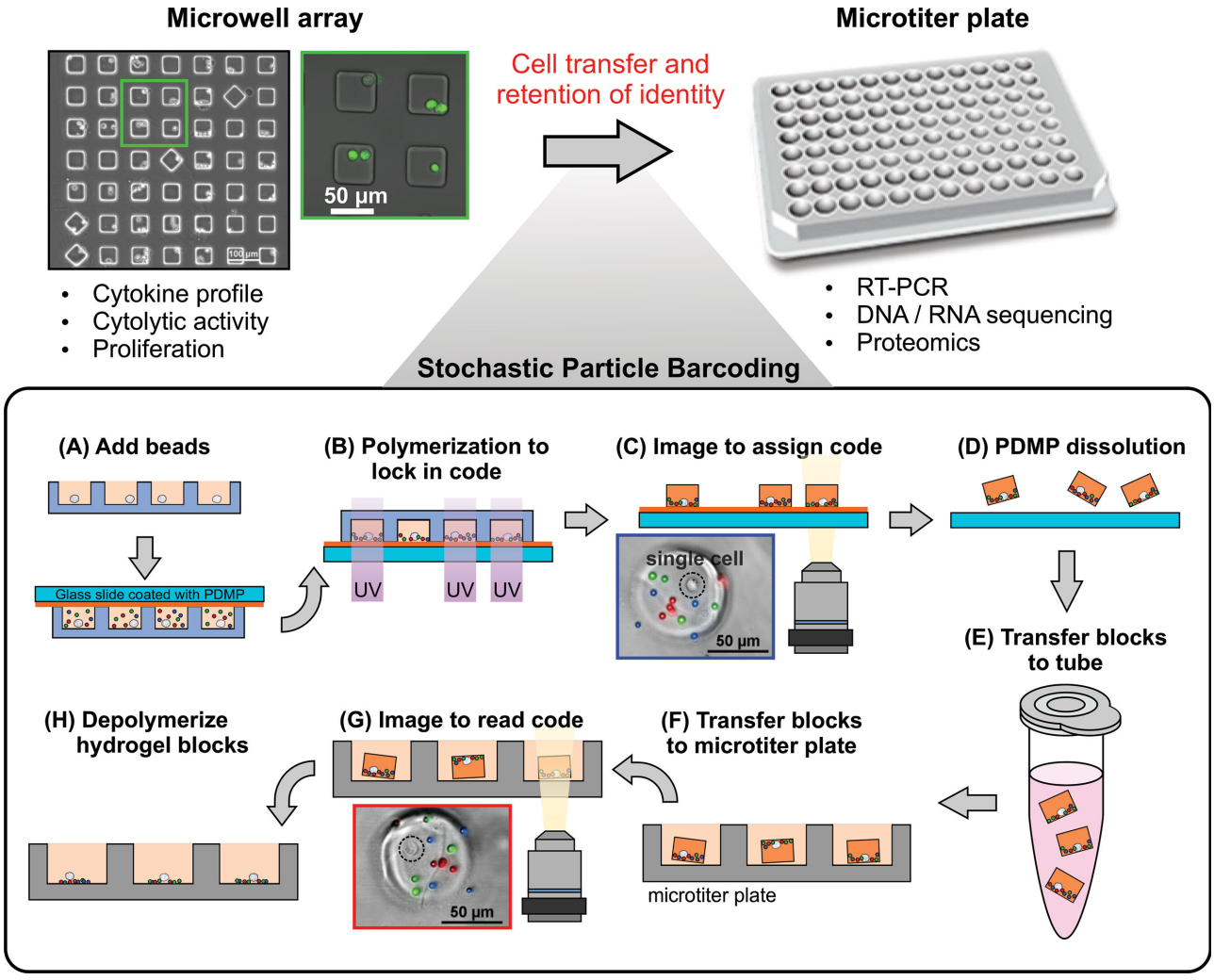

Figure 1. A schematic overview of the stochastic particle barcoding (SPB) method. A) Addition of PEGDA polymer solution with fluorescent beads into microwell array and sealing with glass slide coated with PDMP. B) Encapsulation of all or selected (shown) microwells by photopoylmerization of the hydrogel. Encapsulated beads constitute a random code based on their color, number, and relative positions. C) Removal of glass slide with polymerized blocks and imaging of the blocks to assign the code. D) Resuspension of hydrogel blocks attached to the cover glass slide after uncapping the PDMS microwell array via dissolution of the PDMP sacrificial layer. E) Transfer of resuspended blocks into a tube. F) Transfer of blocks into a microtiter plate by serial dilution. G) Imaging blocks after transfer to read the code. H) Digestion of hydrogel blocks to release encapsulated cells.

We compared the matrices associated with each block from the first and second set of images and performed a global optimization to obtain the best set of matches. Each block from the first set of images was compared to each block from the images after transfer by applying different transformations (translation, rotation, and flipping) to computationally identify the best overlap of the beads in the two blocks (Figure 2B). Each comparison of these transformations was scored via a measure of the bead distances between the two blocks, adding a penalty for missing or extra beads, and then recording the minimal score (Figure 2C). We generated a score matrix by finding the minimal scores for each block comparison. A global optimization was then applied to this score matrix (Hungarian algorithm script from Matlab) to obtain a matching matrix that contained the best estimates for block matching, thus recovering block identity (Figure 2C).

To assess the overall accuracy of the block-matching process, we created sets of 100 blocks containing B16F10 cells, transferred them from a microwell array (MWA) to microtiter plates, and compared matches via the imaging algorithm versus ground-truth manual scoring. From the MWA, we first selectively photopolymerized wells containing cells of interest (**Figure 3**A). Direct UV writing with a fully motorized microscope was used to selectively photopolymerize microwells; this hardware had sufficient throughput for selecting 100's of single cells. To increase throughput even further, it should be possible to employ micromirror arrays (DMDs)[34] to selectively photopolymerize a large number of selected microwells en masse. We also note that photopolymerization is not restricted to microwells; any shape and even isolated sets of cells can be encapsulated in photopolymer blocks.

When removing the glass slide from the MWA, only the contents of the selected wells were transferred to the cover glass slide (Figure 3B); we then imaged the hydrogel blocks to assign a code to each block. We imaged the individual blocks again after transfer to a microtiter plate (Figure 3C).

www.MaterialsViews.com

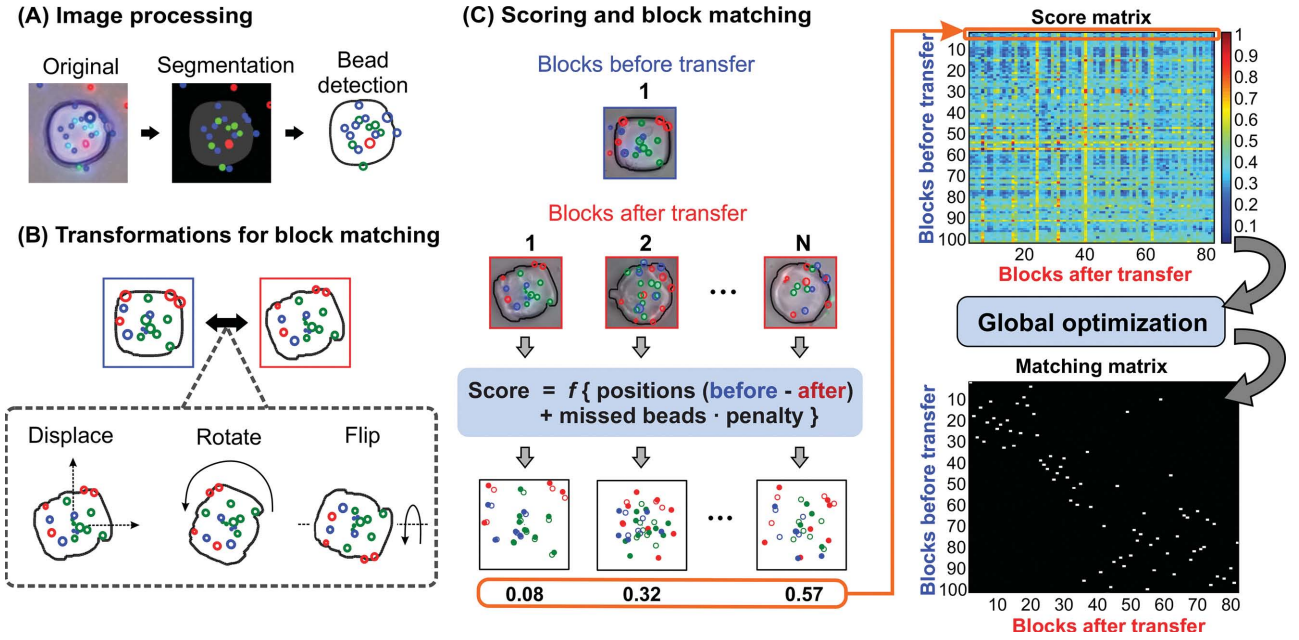

Figure 2. Image correlation process for block identity recovery. A) Images were first processed to contour the blocks and detect beads in the blocks, thus generating the code. B) To match the processed block codes, we applied transformations (i.e., 2D displacement, rotation and flip) during the image correlation process. C) To perform the correlation, we compared the bead positions between the before/after image codes while applying the transformations in (B) to one of the blocks. (Here we show the actual images, but the processing was on the extracted codes). Each pre-transfer block image was compared to all the images from the blocks after transfer, from which we generated the score matrix. Finally, we used the Hungarian algorithm to determine the global set of best image matches and generate the matching matrix to recover block identity.

Figure 3D shows three sets of experiments using a bead concentration that yielded an average of 15 beads per block. Images of individual blocks were processed to determine bead information (i.e., location and color) for block comparison. Figure S2 demonstrates the block matching process, showing a subset of blocks and the associated matching scores. Comparing the computational analysis with manual inspection, the block-matching accuracy of this process for individual experiments on 100 blocks ranged from 93–98%, with an average accuracy of 96%. By manual image inspection of the matching errors, we identified two main sources of error during the identification process (Supporting Information, Figure S3): (i) Residual free-floating beads that can attach to the glass substrate near blocks and are mistakenly identified as part of that block (Figure 1C), leading to an overestimation of the number of beads per block. Washing mitigates this source of error, and it is conceivable that alternative surface functionalization of the beads could reduce this even further. (ii) Bead clusters are sometimes mistakenly segmented into single large beads during image processing, which can be addressed with more sophisticated segmentation or heuristics. Overall, our results demonstrate that the approach for random coding is feasible and can attain useful accuracy.

The total time for photopolymerization, initial barcode imaging, transfer to the second assay, and re-imaging of blocks averaged ~3 hrs per 100 blocks. The most time-consuming steps in the SPB process are the imaging steps (Figures 1C and 1G) and the code matching process. However, imaging throughput could be increased by optimizing the imaging steps (i.e., magnification, numerical aperture, and camera resolution to maximize the number of blocks imaged/time). Additionally, since matching can be performed offline after the experiment is completed, its throughput needs are secondary.

2.3. Modeling the SPB Process

We developed a Monte Carlo model of the SPB process to understand how the accuracy of the block matching process is affected by different parameters of the method (i.e., bead number, missing beads, number of colors, block loss, etc.). The model computationally generated different numbers of blocks of a given size and with probabilistic distributions of the number, color and 2D locations of beads to simulate the first set of images from the blocks before transfer (Supporting Information, Figure S4A). Then, the model applies the same transformations that we experimentally observed occurring to the transferred blocks (i.e., bead loss, bead movement within the block, block loss during the transfer process), producing a second set of images. The magnitude and distributions of those transformations were empirically derived from the experiments (Supporting Information, Figure S4B).

The Monte Carlo model was first used to computationally generate a series of 100 blocks to examine the importance of using bead location in the code relative to just using bead number and color. As expected, the model showed increasing matching accuracy as the average number of beads per block (k) increased (**Figure 4**A). More interestingly, we observed dramatic improvement in block matching accuracy when bead location was used as part of

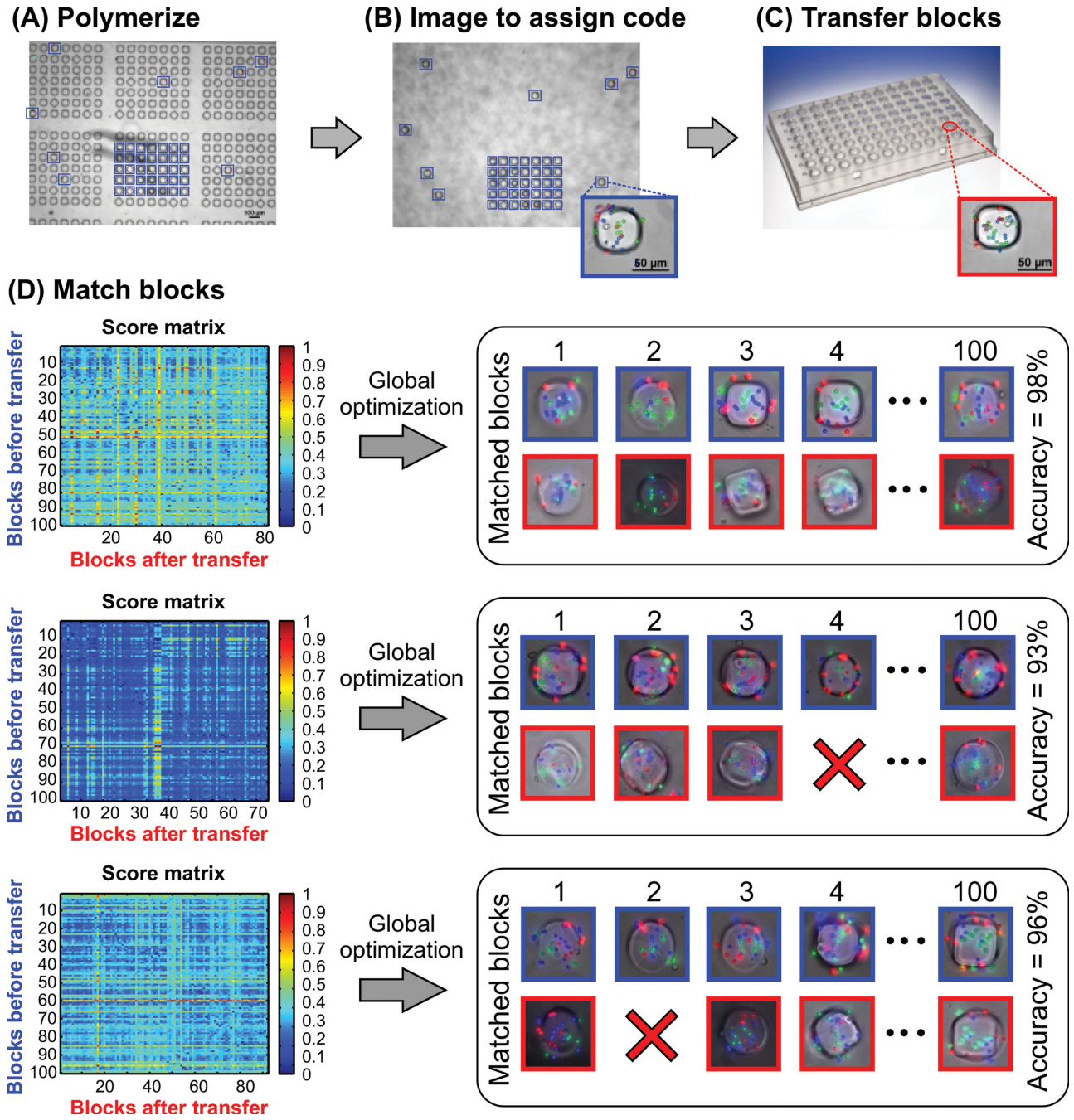

Figure 3. SPB encapsulation and block matching. (A-C) Representative images of blocks during different steps of the SPB method, including A) polymerization, B) removal of the sealing glass slide with polymerized blocks from the microwell array, and C) block transfer to microtiter plate. D) Block-matching accuracy from three 100-block experiments, with an overall accuracy of 96±2%. The blue framed images show the individual blocks before transfer, and the red framed images show the best candidate predicted by our custom block matching software. Red "X"'s refer to incorrect matches.

the code rather than just the number and color of beads (Figure 4A). For example, considering 100 blocks that need to be matched without any bead or block loss, an average of 6 beads per block was sufficient to obtain 0.1% matching error using bead location, number, and color as the code. In contrast, using only bead number and color required ~40 beads per block to obtain a 1% error. Bead color was also important. Using three colors instead of one substantially improved block matching accuracy (Supporting Information, Figure S5A), though it did not have as strong an influence as the location of the beads.

Beads can be lost (or gained) during block transfer, which subsequently affects accuracy. Comparing simulations where blocks can lose up to 25% of the beads in the block before transfer to simulations without any bead loss, we found a modest increase in the average number of beads per block was needed to maintain 0.1% error in block matching (i.e., two additional beads per block, Supporting Information Figure S5B).

www.MaterialsViews.com

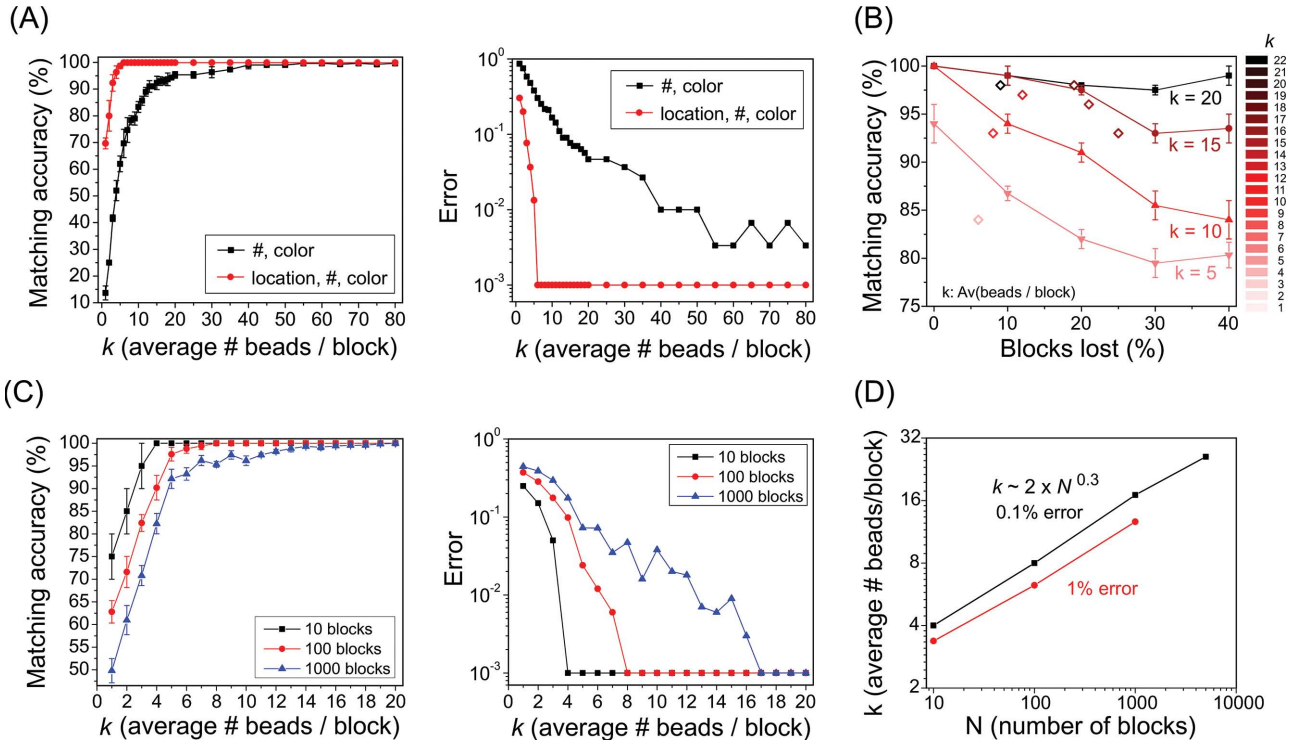

Figure 4. SPB modeling. A) Simulations of the matching accuracy and error (1-accuracy) for $N = 100$ blocks (n = 3, no bead loss and no block loss), when using bead color, number, and location (red) or no location (black) in the code. B) Simulations (lines, n = 5) and experimental results (◊, n = 7 experiments) varying block loss and average number of beads per block, k ($N = 100$ blocks). C) Simulations of matching accuracy and error for $N = 10$, 100 and 1000 blocks (n = 3, bead loss up to 25% of k, bead movement up to 5 μm, and no block loss). D) Summary of the scalability of SPB showing the k needed to obtain 0.1% and 1% error in block matching for various N.

A more significant experimental parameter was the loss of blocks during the transfer process (either due to loss during pipetting or imaging failures). The model predicts that block matching accuracy decreases substantially with increasing block loss for small k values (Figure 4B). For example, matching accuracy for $k = 5$ beads per block, falls from 94% to 83% when increasing the percentage of blocks lost from 0% to 20%, respectively. The loss in matching accuracy becomes less important as k increases, and interestingly, the accuracy becomes insensitive to block loss for $k \geq 15$ beads per block (99% to 97% accuracy for $k = 15$ for 0% of blocks lost and 20%).

To assess the validity of the model, we performed matching experiments with different values for k and amount of block loss, superimposing experimental results onto simulation results (Figure 4B). We found that experiments qualitatively and quantitatively tracked the predictions from modeling. For instance, comparing the accuracies of block matching from the experimental results (96%) and the model (97%) for $k = 15$ beads per block, with a 21% block loss and <25% bead loss, the relative difference between experiment and simulation was about 1%. These results confirm that increasing k (average number of beads per block) by 1 obtains high accuracies in block matching and good protection against the effects of block loss and bead loss. Thus, experimentally, one can improve desired performance by adding more beads/block, decreasing the loss of blocks during the procedure, or both.

One important criterion for a cell tracking method is scalability. The ideal method should be scalable to track thousands of unique blocks, beyond the limit that most current single-cell analysis tools can handle.[35,36] We simulated scale-up of the SPB method and found, as expected, increasing average number of beads per block, k, is required to track increasing numbers of blocks to maintain a given accuracy (Figure 4C). We found that the required k scales approximately as $2 \times N^{0.3}$, where N is the number of blocks, suggesting that ~32 beads/block would be needed to track 10,000 blocks with a 0.1% matching error (Figure 4D). This scaling is quite favorable, and can be improved even further by increasing the number colors,[26] adding parameters to the code (bead size, for example), or decreasing desired accuracy.

2.4. Viability of Cells and Recovery of Cellular Biomacromolecules from Barcoded Blocks

As the final step in optimizing the SPB workflow, we iterated process variables that could affect cell viability during processing and recovery from hydrogel blocks. Viable cell isolation is crucial for the recovery of usable biological materials for downstream assays and single-cell or clonal growth, which are of broad interest for many biological applications, such as selecting yeast and bacteria for bioproduction,[37,38] and the analysis of various clonal populations in biology, such as B[39–41] and T cells[42] in immunology or circulating tumor cells in

small NANO MICRO

oncology.[43] Notably, MWAs have been used to screen and clone cells, but the upper limit has remained approximately 100 cells per array by a manual recovery method.[10,18,36] Conceivably, every well within the MWA could be encapsulated and isolated in a single workflow using SPB, providing an order of magnitude increase in the absolute number of events and reducing process time. We determined optimal conditions for SPB by quantifying the effects of photoinitiator concentration and UV exposure on cell viability. A murine melanoma cell line (B16F10) was used as a model cell type, and we found that photoinitiator concentrations up to 0.5% for 1 h still retained approximately 80% viability (**Figure 5**A, left). Typically, the UV exposure time required to achieve single well photopolymerization at this photointiator concentration is 30 s to 1 min. We studied the compound effect of UV exposure for 2 min (twice the typical required time) and found that viability was maintained at approximately 50% in 0.5% Irgacure (Figure 5A, right). Thus, we kept these conditions (0.5% photoinitiator) as a compromise between cell viability and photpolymerization time (30 s UV exposure/photopolymerization time). Finally, we photopolymerized hydrogel blocks with single cells, then manually picked blocks for collagenase digestion and subsequent clonal outgrowth. We successfully isolated B16F10 cells that retained their ability to grow and adhere after undergoing the entire SPB and recovery method (Supporting Information, Figure S6). This result indicates that clonal populations can readily be selected, isolated, and grown out, greatly increasing the potential throughput for functional screening and subsequent cloning applications of the MWA platform.

SPB has the potential to enable integration of information on phenotypes obtained from microsystems (here, MWAs) with downstream applications (e.g., polymerase chain reaction, PCR; reverse transcription PCR, RT-PCR; clonal

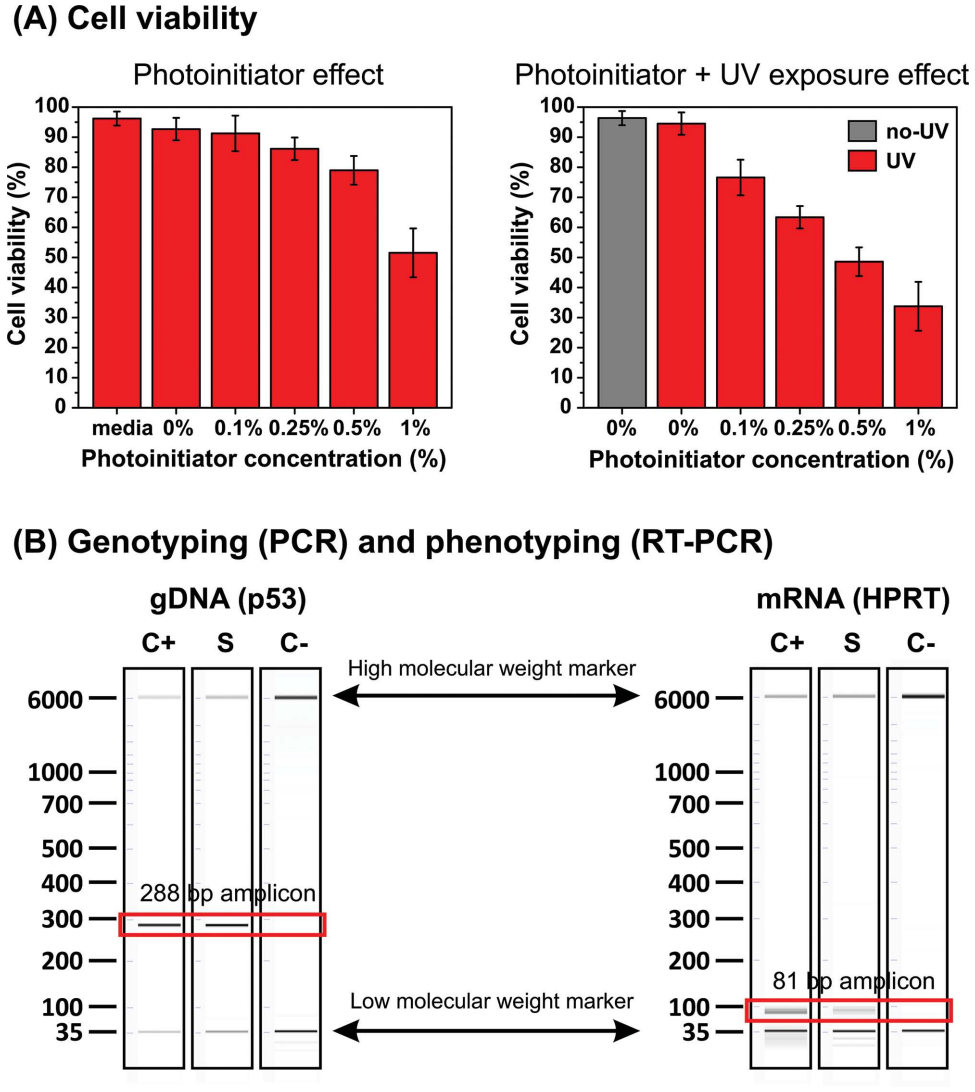

Figure 5. Recovery of nucleic acids and viable cells from stochastic barcoded, enzyme-degradable PEGDA blocks. A) Viability of B16F10 cells following 1 h exposure to indicated concentrations of photoinitiator (up to 1%; left) or 1 h exposure to photoinitiator with 2 min exposure to UV (right). Bars represent average and whiskers represent standard deviation; $n = 2$. B) Capillary electrophoresis and digital gel results for p53 (left) and HPRT (right) following PCR of genomic DNA and RT-PCR of total RNA, respectively, isolated from PEGDA-encapsulated B16F10 cells. Expected amplicon sizes indicated. Lanes: C+, B16F10 cells; S, cell-laden PEGDA blocks; C-, empty PEGDA blocks.

isolation and derivation). Many biological questions revolve around heterogeneity at the genetic level, and researchers often rely on these downstream analytical tools. To determine the suitability of the SPB process for isolating DNA and RNA following single-cell analytical analysis, we seeded MWAs with B16F10 cells at densities of approximately 1 cell per microwell. Subsequently, we photopolymerized blocks with acrylate-PEG-peptide-PEG-acrylate containing a collagenase-sensitive peptide sequence (GGGPQGIWGQGK), and used an automated micromanipulator to visually verify and transfer only hydrogel blocks with known contents (either empty or encapsulated single cells) into 96-well plates. Empty blocks served as negative controls and non-encapsulated cells were used as positive controls. All samples were processed in parallel with the same regimen of collagenase digestion and cellular lysis. Magnetic beads were added during lysis to capture nucleic acids released from the lysed cells, and beads were then processed to isolate genomic DNA or total RNA as described by the manufacturer's protocols.

To evaluate the ability of SPB to recover intact DNA from coded cells, we again used a micromanipulator to manually identify and collect groups of 5–10 blocks with single cells. We then recovered total genomic DNA from digested blocks and transferred their content to microtiter plates containing a PCR reaction mixture with primers targeting a 288 base pair (bp) region of the gene encoding p53, the most commonly mutated tumor suppressor gene in human cancers.[44] As demonstrated in Figure 5B, left, digestion of hydrogel blocks containing single B16F10 cells (**lane S**) produced a band of equivalent size as that generated from non-encapsulated cells used as a positive control (**lane C+**); digestion of hydrogel blocks without cells produced no bands (**lane C-**) indicating that the photopolymerization solution itself does not contain amplifiable genomic DNA (e.g., free DNA from dead cells).

RT-PCR is another commonly used assay that examines the expression level of genes within cells to phenotype gene regulatory networks. We examined the integrity of hypoxanthine guanine phosphoribosyl transferase (*HPRT*) mRNA for use in RT-PCR analyses. *HPRT* is a housekeeping gene frequently used to normalize RNA input in RT-PCR reactions, and is less abundant compared to other housekeeping genes such as glyceraldehyde-3-phosphate dehydrogenase.[45] Blocks were isolated manually again via micromanipulator followed by hydrogel block digestion and cell lysis as described above. Using exon-spanning primers designed for real time RT-PCR, we achieved successful amplification of *HPRT* mRNA (Figure 5B, right) from positive control cells (**lane C+**) and digested hydrogel blocks containing single cells (**lane S**) with no products detected in digested, empty hydrogel blocks (**lane C-**). Both PCR and RT-PCR on encapsulated cells were successfully performed in 4 independent experiments; no failed reactions occurred when the encapsulated cells were visually confirmed by microscopy.

3. Conclusion

We have introduced stochastic particle barcoding as a simple and scalable method for tracking cell identity across analytical platforms. We developed software to recover the identity of blocks and thus encapsulated cells after transferring between analytical platforms, with matching accuracy that was consistent and in agreement with simulations from a Monte Carlo model. The model also showed that SPB scales favorably with the number of beads per block for larger populations of blocks. Finally, we showed that we can recover the cells by digesting the transferred polymer blocks with collagenase, and successfully recovered cells for genotyping, phenotyping, and clonal outgrowth. SPB therefore should enable the performance of multiparametric studies in sparse cell populations to improve our understanding of cellular heterogeneity across diverse biological fields and enhances the utility of many lab-on-a-chip type platforms.

4. Experimental Section

PDMP-Coated Glass Slides: poly(2,2-dimethoxy nitrobenzyl methacrylate-r-methyl methacrylate-r-poly(ethylene glycol) methacrylate) (PDMP) was used a pH sensitive degradable sacrificial layer on top of the sealing glass slides for the PDMS microwell arrays. PDMP was synthetized according to the protocols described in.[33] APTES glass slides (75 × 25 mm^2, 1 mm Thick, Surface Coated with APTES, Electron Microscopy Sciences) were spin coated adding 90 µL of a 7.5 wt% PDMP solution in 1,4-dioxane (Sigma-Aldrich) and spinning at 2000 rpm for 2 min. PDMP-coated slides were dried in vacuum overnight to enhance adhesion, and then exposed to ultra-violet (UV) light for 2 min (15 mW cm^{-2} at 240–395 nm) to render the PDMP layer pH sensitive.[33] Results from profilometer analysis (Dektak 150, Veeco) showed that the resulting PDMP layer was 150 nm thick (Supporting Information, Figure S7).

PEGDA: Pre-polymer solutions containing 20% w/v 1 KDa PEGDA (Laysan Bio) and 1% catalase (Sigma) as anti-oxidant to improve cell viability and enhance photopolymerization were prepared in Hank's buffered saline solution (Gibco) adjusted to pH 6 with hydrochloric acid (HCl) . The solution was then vortexed and filtered with 0.8 µm PTFE filter (National Scientific).

Degradable Peptide-PEGDA: Synthesis of peptide-PEGDA MW 8000 was done by reacting acrylate-PEG-Succinimidyl Valerate (acrylate-PEG-SVA MW 3,400 Da, Laysan Bio) with the proteolytically degradable peptide sequence (GGGPQGIWGQGK), similarly as described in ref [30]. A solution of 1% catalase was prepared using HBSS at pH 6, vortexed and filtrated with 0.2 µm PTFE filter. Then, the pre-polymer solution of peptide-PEGDA was prepared using this filtered catalase solution, 20% w/v peptide-PEGDA MW 8,000.

Pre-polymer Solution for Cell Encapsulation: Consists of a mixture of 80% v/v PEGDA and 9% v/v degradable peptide-PEGDA of previous pre-polymer solution, 0.5% w/v photoinitiator (Irgacure 2959, Ciba), 4.4% v/v methanol, 6.6% v/v mixture of RGB fluorescent polystyrene latex 4.5 um beads at a concentration 5×10^8 particles mL^{-1} (Fluoresbrite Microspheres YO-YG-BB, Polyscience Inc.).

Cells: B16F10 murine melanoma cells were cultured at 37 °C in 5% CO2 and 95% relative humidity. Cells were passaged every 2–3 days in Dulbecco's Modified Eagle Medium (DMEM) supplemented with 10% fetal bovine serum and penicillin/streptomycin. Healthy human peripheral blood mononuclear cells were

obtained from Research Blood Components (Brighton, MA) under a protocol exemption approved by the Committee on the Use of Humans as Experimental Subjects at MIT. Briefly, healthy human peripheral blood was centrifuged for 25 min at room temperature over a density gradient (Ficoll-paque PLUS; GE Healthcare Life Sciences). PBMCs were harvested and used fresh in RPMI1640 supplemented as above or frozen in 90% FBS/10% DMSO for future use.

Microwell Arrays: Arrays of microwells comprising 50 μm cubic wells (84,672 wells/array) were prepared on 75 × 25 mm^2 glass slides (Corning) following previously reported protocols.[21] To fabricate the arrays, the silicone elastomer poly(dimethylsiloxane) (PDMS) (Sylgard 184 Silicone Elastomer Kit, Dow Corning,) was mixed at a 10:1 ratio of base:catalyst, degassed under a vacuum at room temperature for 1 h, and then injected into a mold containing a microfabricated silicon master. The PDMS was cured at 80 °C for 4 h and subsequently released from the mold to produce a glass slide-backed array of microwells. Shortly before use, the arrays of microwells were treated with oxygen plasma (Plasma Cleaner PDC-001, Harrick Plasma) for 15 min to sterilize the array, turn the PDMS hydrophilic, and oxidize the array surface to enhance photopolymerization of PEGDA hydrogels.

Cell Encapsulation and Block Imaging: Microwells containing cells of interest and pre-polymer solution with beads are photopolymerized by direct UV writing using Nikon Eclipse TiE inverted microscope fitted with a florescent light source (X-Cite 120, EXFO), an UV-2E/C excitation filter block (Nikon), and Photometrics CoolSnap HQ2 CCD camera. The combination of a 40X magnification (CFI S Plan Fluor ELWD 40X objective, Nikon) combined with a diaphragm allows to adjust the UV exposure area to the size of a single microwell (i.e., 65 × 65 $μm^2$). Automated XY motorized stage (BioPrecision2, Ludl Electronics) permits to move along the MWA photo-polymerizing only those microwells with the cells of interest. Polymerization time for given photoinitiator concentration is about 30 s for a given UV light intensity of 20 mW cm^{-2} (measured with UVA meter, Control Company). Microscope and its parts were controlled with NIS-Elements Ar software (Nikon). Images of the blocks before and after transfer into the microtiter plates were done with same microscope and objective using filter sets UV-2E/C (Nikon), ET GFP and ET dsRED (Chroma), controlled with same previous software.

Manual Block Recovery via Capillary Micromanipulator: An AVISO CellCelector robot (Automated Lab Solutions, software version 2.8; Jena, Germany) was used for picking of hydrogel cubes. A 96-well plate containing polymer cubes was placed on the deck of the microscope. The CellCelector software was then used for real time visualization and selective recovery of single-cell cubes. A glass capillary with an opening of approximately 150 μm was used to aspirate 1 μL of culture medium, then an additional 1 μL was aspirated to pick up each cube. Cubes were deposited into a 96-well collection plate, and the tool sensor was used to ensure that the tip touched to the bottom of the plate and that the entire 2 μL volume was dispensed. Borosilicate glass capillaries with an outer diameter of 1.5 mm and an inner diameter of 0.86 mm were pulled on the Sutter Instruments Flaming/brown micropipette puller, model P-1000 (Novato, California).

Polymer Digestion: Transferred blocks with cells were digested with filtered collagenase Type 1 (Worthington Biochemical Corp.) by adding 1/4 of the total sample volume at 4000–8000 U mL^{-1} for 10–20 min at room temperature (agitation at 37 °C enhance polymer digestion). The digestion reaction was stopped by addition of 2X volume HBSS with 10 mM EDTA.

Nucleic Acid Isolation: Cells were lysed in 1x MagMAX Lysis/Binding Solution (Life Technologies) in the presence of Agencourt AMPure XP magnetic beads (Beckman Coulter, Inc.) for gDNA isolation OR MagMAX-96 Total RNA Binding Beads (Life Technologies) for total RNA isolation. The lysis solution was mixed well and incubated under agitation/rotation for 5 min at room temperature. Beads were washed as described in the manufacturer's protocol for gDNA or RNA, using either a magnetic plate holder (Biotek) or microcentrifuge tube stand (Life Technologies) to retain beads during washes. RNA was digested with TurboDNase at room temperature for 15 min to remove contaminating gDNA. gDNA was eluted using Endofree TE (Qiagen) and RNA was eluted using the supplied MagMAX Elution Buffer (Life Technologies) followed by pipetting up and down to resuspend beads. Beads were immobilized magnetically as previously described and supernatants were transferred to DNA Lobind tubes (Eppendorf).

PCR and RT-PCR: Primer sequences for p53 PCR were A: 5′ CAC AAA AAC AGG TTA AAC CCA G 3′ and B: 5′ AGC ACA TAG GAG GCA GAG AC 3′. Primers for *HPRT* mRNA were obtained from Life Technologies (Assay Mm01545399_m1) as a premixed 20x concentrated Taqman solution for real time RT-PCR. PCR (Platinum Taq, Life Technologies) and OneStep RT-PCR (Qiagen) master mixes were directly added to total eluted gDNA or RNA. PCR cycling parameters: 94 °C for 2 min followed by 45 cycles (94 °C for 30 s, 58 °C for 1 min, 68 °C for 1 min), followed by 72 °C for 5 min. RT-PCR cycling parameters: 50 °C for 30 min, 95 °C for 15 min followed by 45 cycles (94 °C for 1 min, 60 °C for 1 min, 72 °C for 1 min) followed by 72 °C for 10 min. Reaction products were stored at 4 °C and subsequently analyzed using an Agilent Bioanalyzer capillary electrophoresis system using DNA High Sensitivity assay (Agilent, Santa Clara, CA).

Supporting Information

Supporting Information is available from the Wiley Online Library or from the author.

Acknowledgements

M. Castellarnau and G. L. Szeto contributed equally to this work. This work was supported through the Ragon Institute of MGH, MIT, and Harvard. We would like to thank Prof. Junsang Doh for providing the polymer PDMP, Rachel M. Barry for assistance with single block/single cell isolation via CellCelector, and the MIT BioMicro center for analytical runs on the Agilent Bioanalyzer. This work was also supported in part by the Koch Institute Support (core) grant P30-CA14051 from the National Cancer Institute. GLS is supported by the National Institutes of Health under Ruth L. Kirschstein National Research Service Award #1F32CA180586. JCL is a Camille Dreyfus Teacher-Scholar. DJI is an investigator of the Howard Hughes Medical Institute.

[1] J. C. Love, *AIChE J.* **2010**, *56*(10), 2496–2502.
[2] M. B. Elowitz, A. J. Levine, E. D. Siggia, P. S. Swain, *Science* **2002**, *297*(5584), 1183–1186.
[3] E De Sousa, F. Melo, L. Vermeulen, E. Fessler, J. P. Medema, *EMBO Rep.* **2013**, *14*(8), 686–695.
[4] S. L. Spencer, S. Gaudet, J. G. Albeck, J. M. Burke, P. K. Sorger, *Nature* **2009**, *459*(7245), 428–432.
[5] K. Liddiard, M. Rosas, L. C. Davies, S. A. Jones, P. R. Taylor, *Eur. J. Immunol.* **2011**, *41*(9), 2503–2508.
[6] H. Katayama, Y. Hattori, K. Ogata, H. Yan, E. Satoh, K. Teramoto, S. Arii, R. Kamide, H. Nakagawa, H. Kimura, *Transplantation Proc.* **2005**, *37*(1), 17–19.
[7] F. S. O. Fritzsch, C. Dusny, O. Frick, A. Schmid, *Annu. Revi. Chem. Biomolec. Engineering* **2012**, *3*(1), 129–155.
[8] J. C. Love, J. L. Ronan, G. M. Grotenbreg, A. G. van der Veen, H. L. Ploegh, *Nature Biotechnol.* **2006**, *24*(6), 703–707.
[9] N. Yoshimoto, A. Kida, X. Jie, M. Kurokawa, M. Iijima, T. Niimi, A. D. Maturana, I. Nikaido, H. R. Ueda, K. Tatematsu, K. Tanizawa, A. Kondo, I. Fujii, S. i. Kuroda, *Sci. Rep.* **2013**, *3*, 1191.
[10] N. Varadarajan, D. S. Kwon, K. M. Law, A. O. Ogunniyi, M. N. Anahtar, J. M. Richter, B. D. Walker, J. C. Love, *Proc. Natl. Acad. Sci. USA* **2012**, *109*(10), 3885–3890.
[11] C. Ma, R. Fan, H. Ahmad, Q. Shi, B. Comin-Anduix, T. Chodon, R. C. Koya, C.-C. Liu, G. A. Kwong, C. G. Radu, A. Ribas, J. R. Heath, *Nat. Med.* **2011**, *17*(6), 738–743.
[12] J. Wang, H. C. Fan, B. Behr, S. R. Quake, *Cell* **2012**, *150*(2), 402–412.
[13] H. C. Fan, J. Wang, A. Potanina, S. R. Quake, *Nature Biotechnol.* **2010**, *29*(1), 51–57.
[14] A. K. White, M. VanInsberghe, O. I. Petriv, M. Hamidi, D. Sikorski, M. A. Marra, J. Piret, S. Aparicio, C. L. Hansen, *Proc. Natl. Acad. Sci. USA* **2011**,*108*(34),13999–14004.
[15] E. Brouzes, M. Medkova, N. Savenelli, D. Marran, M. Twardowski, J. B. Hutchison, J. M. Rothberg, D. R. Link, N. Perrimon, M. L. Samuels, *Proc. Natl. Acad. Sci. USA* **2009**, *106*(34), 14195–14200.
[16] K. Leung, H. Zahn, T. Leaver, K. M. Konwar, N. W. Hanson, A. P. Pagé, C.-C. Lo, P. S. Chain, S. J. Hallam, C. L. Hansen, *Proc. Natl. Acad. Sci. USA* **2012**, *109*(20), 7665–7670.
[17] H. N. Joensson, H. Andersson Svahn, *Angew. Chem. Int. Ed.* **2012**, *51*(49), 12176–12192.
[18] J. H. Choi, A. O. Ogunniyi, M. Du, M. Du, M. Kretschmann, J. Eberhardt, J. C. Love, *Biotechnol. Progress* **2010**, *26*(3), 888–895.
[19] P. O. Krutzik, G. P. Nolan, *Nat. Meth.* **2006**, *3*(5), 361–368.
[20] S. P. Perfetto, P. K. Chattopadhyay, M. Roederer, *Nat. Rev. Immunol.* **2004**, *4*(8), 648–655.
[21] Y. J. Yamanaka, G. L. Szeto, T. M. Gierahn, T. L. Forcier, K. F. Benedict, M. S. N. Brefo, D. A. Lauffenburger, D. J. Irvine, J. C. Love, *Analyt. Chem.* **2012**, *84*(24), 10531–10536.
[22] D. Dendukuri, D. C. Pregibon, J. Collins, T. A. Hatton, P. S. Doyle, *Nat. Mater.* **2006**, *5*(5), 365.
[23] P. Mali, J. Aach, J.-H. Lee, D. Levner, L. Nip, G. M. Church, *Nat. Meth.* **2013**, *10*(5), 403–406.
[24] B.-K. Oh, J.-M. Nam, S. W. Lee, C. A. Mirkin, *Small* **2006**, *2*(1), 103–108.
[25] S. Alon, F. Vigneault, S. Eminaga, D. C. Christodoulou, J. G. Seidman, G. M. Church, E. Eisenberg, *Genome Res.* **2011**, *21*(9), 1506–1511.
[26] S. Fournier-Bidoz, T. L. Jennings, J. M. Klostranec, W. Fung, A. Rhee, D. Li, W. C. W. Chan, *Angew. Chem. Int. Ed.* **2008**, *47*(30), 5577–5581.
[27] D. Peck, E. Crawford, K. Ross, K. Stegmaier, T. Golub, J. Lamb, *Genome Biol.* **2006**, *7*(7), R61.
[28] D. K. Wood, G. B. Braun, J. L. Fraikin, L. J. Swenson, N. O. Reich, A. N. Cleland, *Lab Chip* **2007**, *7*(4), 469–474.
[29] E. Fernandez-Rosas, R. Gómez, E. Ibañez, L. Barrios, M. Duch, J. Esteve, C. Nogués, J. A. Plaza, *Small* **2009**, *5*(21), 2433–2439.
[30] S.-H. Lee, J. S. Miller, J. J. Moon, J. L. West, *Biotechnol. Progress* **2005**, *21*(6), 1736–1741.
[31] J. Doh, D. J. Irvine, *J. Am. Chem. Soc.* **2004**, *126*(30), 9170–9171.
[32] J. S. Katz, J. Doh, D. J. Irvine, *Langmuir* **2005**, *22*(1), 353–359.
[33] M. Kim, J.-C. Choi, H.-R. Jung, J. S. Katz, M.-G. Kim, J. Doh, *Langmuir* **2010**, *26*(14), 12112–12118.
[34] A. P. Zhang, X. Qu, P. Soman, K. C. Hribar, J. W. Lee, S. Chen, S. He, *Adv. Mater.* **2012**, *24*(31), 4266–4270.
[35] P. K. Chattopadhyay, T. M. Gierahn, M. Roederer, J. C. Love, *Nat. Immunol.* **2014**, *15*(2), 128–135.
[36] A. O. Ogunniyi, C. M. Story, E. Papa, E. Guillen, J. C. Love, *Nat. Protocols* **2009**, *4*(5), 767–782.
[37] V. Panagiotou, K. R. Love, B. Jiang, J. Nett, T. Stadheim, J. C. Love, *Appl. Environm. Microbiol.* **2011**, *77*(9), 3154–3156.
[38] K. R. Love, T. J. Politano, V. Panagiotou, B. Jiang, T. A. Stadheim, J. C. Love, *PLoS ONE* **2012**, *7*(6), e37915.
[39] Y. Weiss-Ottolenghi, J. M. Gershoni, *FEBS Lett.*. **2014**, *588*(2),318–325.
[40] C. Q. Nguyen, A. O. Ogunniyi, A. Karabiyik, J. C. Love, *PLoS ONE* **2013**, *8*(3), e58127.
[41] C. M. Story, E. Papa, C.-C. A. Hu, J. L. Ronan, K. Herlihy, H. L. Ploegh, J. C. Love, *Proc. Natl. Acad. Sci. USA* **2008**, *105*(46), 17902–17907.
[42] J. J. Miles, D. C. Douek, D. A. Price, *Immunol. Cell Biol.* **2011**, *89*(3), 375–387.
[43] D. F. Hayes, C. Paoletti, *J. Internal Medicine* **2013**, *274*(2), 137–143.
[44] M. Olivier, M. Hollstein, P. Hainaut, *Cold Spring Harbor Persp. Biol.* **2010**, *2*(1), a001008.
[45] D. L. Foss, M. J. Baarsch, M. P. Murtaugh, *Animal Biotechnol.* **1998**, *9*(1), 67–78.

Received: May 17, 2014
Revised: July 29, 2014
Published online: September 2, 2014